Progress In Electromagnetics Research C, Vol. 137, 211–222, 2023

Design and Development of CPW-Fed Miniaturized MSA for Improved Gain, Bandwidth and Efficiency Using PRS

Ameet M. Mehta[1, 2, *], Shankar B. Deosarkar[1], and Anil B. Nandgaonkar[1]

Abstract—A Coplanar Waveguide (CPW) fed antenna with a T-type slot and Partially Reflecting Surface (PRS) for gain, bandwidth, and efficiency improvement is presented. The antenna is miniaturized to get size reduction of 46.50%. The miniaturized antenna covers frequencies in C band. The presented antenna structure is easy to design and has size of $0.682\lambda_g \times 0.99\lambda_g \times 0.053\lambda_g$. The PRS with parasitic patches is placed on top of the antenna at a distance of $0.25\lambda_g$. The presented antenna design has a bandwidth of 4.42 GHz (Antenna 1) and 3.87 GHz (Antenna 2) with a percentage bandwidth of 75.81% and 59.58% respectively having average radiation efficiency above 90%. The gains obtained are 7.03 dBi and 6.12 dBi for Antenna 1 and Antenna 2. The gain has < 3 dB variation over the complete band. The obtained results support the design and make the antenna suitable for C band applications.

1. INTRODUCTION

Coplanar Waveguide (CPW) fed slot antennas are used in various applications where size, cost, flexible design, and antenna performance are major restrictions. Generally, all Microstrip Antennas (MSAs) provide narrow bandwidth. The problem with narrow bandwidth antenna is overcome by making slots in the patch and other techniques as studied in [1–4]. CPW antenna provides bidirectional radiation pattern with wide band response. The perimeter of slot ring should be $1.5\lambda_0$, while the perimeter of the feed line is generally λ_0 [5, 6]. Moreover, CPW antenna can be easily fabricated and have less complex structural design.

Many approaches have been studied for miniaturizing MSA, the methods for miniaturization includes half-cutting method [7], using slits [8], using fractal geometry and partial cutting method [9], using shorting post and defected ground structure (DGS) [10]. These methods have significantly contributed to developing compact antennas. The miniaturization of antenna also results in the reduction in gain, bandwidth, and efficiency [11–14].

A number of techniques have been adopted to enhance bandwidth, gain, radiation pattern, and efficiency of an MSA. The technique incorporated should offer benefits like ease in fabrication, less complex, cost effective, improved parameters, etc. In order to achieve these benefits, superstrates like High Impedance Surface (HIS), Frequency Selective Surface (FSS), Reactive Impedance Surface (RIS), partially reflecting surface (PRS), Artificial Magnetic Conductor (AMC), and Electromagnetic Band Gap (EBG) periodic structures are used.

The partially reflecting surfaces with periodic patches over a dielectric substrate have been effectively used as superstrate which results in low profile Resonant Cavity Antenna (RCA) [15–17]. Gain and bandwidth enhancement using PRS with parasitic patches is studied in [18–22]. Use of PRS to get wideband response has been investigated in [23, 24], but the available bandwidth is limited by the

Received 14 July 2023, Accepted 1 September 2023, Scheduled 13 September 2023
* Corresponding author: Ameet M. Mehta (amehta.dbatu@gmail.com).
[1] Department of Electronics and Telecommunication Engineering, Dr. Babasaheb Ambedkar Technological University, Lonere, India.
[2] Department of Electronics and Telecommunication Engineering, Pillai College of Engineering, New Panvel, Raigad, India.

intrinsic characteristics of the magnitude and phase of the reflection characteristics of the PRS designs. Highly directive antenna with PRS placed $\lambda_0/4$ from ground plane has been studied [25]. PRS layer on the single side or double side using single or multiple substrates has been investigated in [26–32], and with PRS patches there is improvement in gain and bandwidth, but the circuit complexity increases.

In this paper, a CPW-fed T-type slot antenna with PRS with parasitic patches on top for improving gain, bandwidth, radiation efficiency, and miniaturization has been proposed. Antenna 1 with PRS with parasitic patches on top yields a bandwidth of 4.42 GHz with percentage bandwidth of 73.36%. Antenna 1 has a gain and average radiation efficiency of 7.03 dBi and 90.40%, respectively. Miniaturized antenna (Antenna 2) with PRS with parasitic patches on top yields a bandwidth of 3.87 GHz with a percentage bandwidth of 59.58%. Antenna 2 has gain and average radiation efficiency of 6.12 dBi and 92.19%, respectively. Antenna miniaturization of 46.50% is achieved. The fabrication and testing of prototype show good consensus in the simulated and measured results.

2. DESIGN OF AN ANTENNA

Antenna 1 geometry is shown in Fig. 1(a). The antenna has dimensions of $1.266\lambda_g \times 0.99\lambda_g \times 0.053\lambda_g$, where λ_g is calculated at the first resonating frequency. The fabrication of antenna is done using an FR4 substrate which has relative permittivity of 4.4 and loss tangent value of 0.02. The benefits of using an FR4 substrate is low cost, wide availability, and easy fabrication. The half side of 'T' type slot has perimeter of $1.44\lambda_g$ which is fed using a CPW feeding structure. The CPW feedline is inductively fed and designed for 50-Ω characteristic impedance. The microstrip feed line has width $W_f = 3\,\text{mm}$ and gap $W_c = 0.5\,\text{mm}$.

$$Z_0 = \frac{Z_{air}}{\sqrt{\varepsilon_e}} \tag{1}$$

where

$$Z_{air} = 60 \ln\left[\frac{F_1 \times h}{w} + \sqrt{1 + \left(\frac{2h}{w}\right)^2}\right] \text{ and } \varepsilon_e = \sqrt{\frac{\varepsilon_r + 1}{2}} \text{ for } w/h \ll 1 \tag{2}$$

Z_0 is the characteristic impedance of the microstrip feed line which is found to be 56.21 Ω. The characteristic impedance is calculated using Equations (1)–(2).

Figure 1(b) shows the equivalent circuit for Antenna 1. Capacitance $Cf1$ is formed between points a and b, i.e., the feed line and the ground plane form two plates of the capacitor, and the gap between the feed line and ground plane acts as dielectric. Similarly, capacitance $Cc1$ is formed between points a and c. Inductance $Lg2$ is formed along the length b-c-d-e. Variations in the value of S_x and S_y vary the values of $Cc1$ and $Lg2$ which results in the change in resonating frequency. Capacitance $Cg1$ is

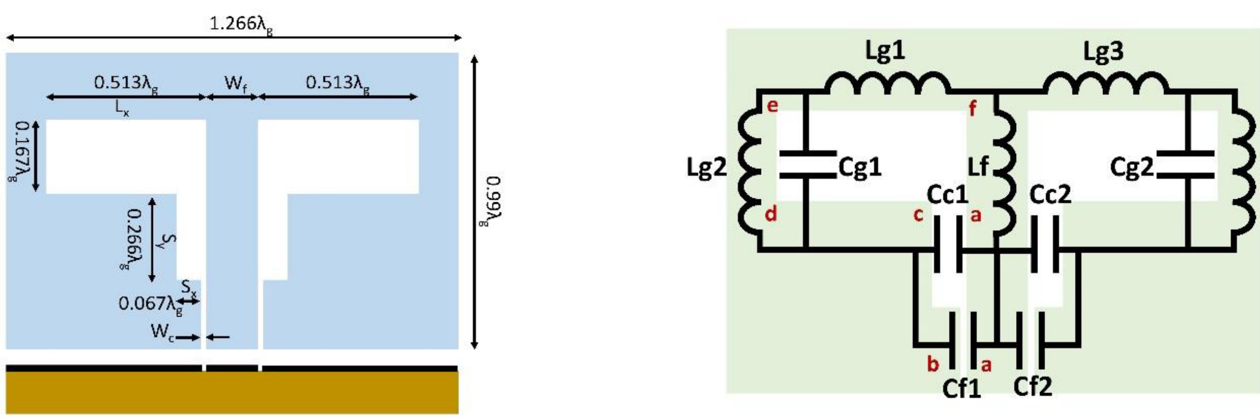

(a) (b)

Figure 1. Antenna design. (a) Antenna 1 geometry, (b) Antenna 1 equivalent circuit.

formed between points d and e, and inductance $Lg1$ is formed along the length e-f. Variations in length L_x varies the values of $Lg1$ and $Cg1$. As the antenna structure is symmetrical capacitances $Cf2, Cc2$, and $Cg2$ are formed similar to $Cf1$, $Cc1$, and $Cg1$, respectively. Inductances $Lg4$ and $Lg3$ are formed similar to $Lg2$ and $Lg1$. Inductance Lf is formed along the length a-f and remains the same for both sides of the structure.

The parametric analysis for Antenna 1 is done by varying the values of S_x, S_y, and L_x. Figs. 2(a), (b), and (c) show S_{11} plot for parametric analysis by varying values of S_x, S_y, and L_x, respectively. When S_x is varied during parametric analysis from 1 mm to 4 mm in step of 1 mm, it is seen that the S_{11} plot shifts upwards completely as S_x increases, and the optimised value of S_x is selected as 2 mm. When the value of S_y is increased during the parametric analysis from 7 mm to 10 mm in step of 1 mm, the S_{11} plot completely shifts downwards, and the optimum value of S_y selected is 8 mm.

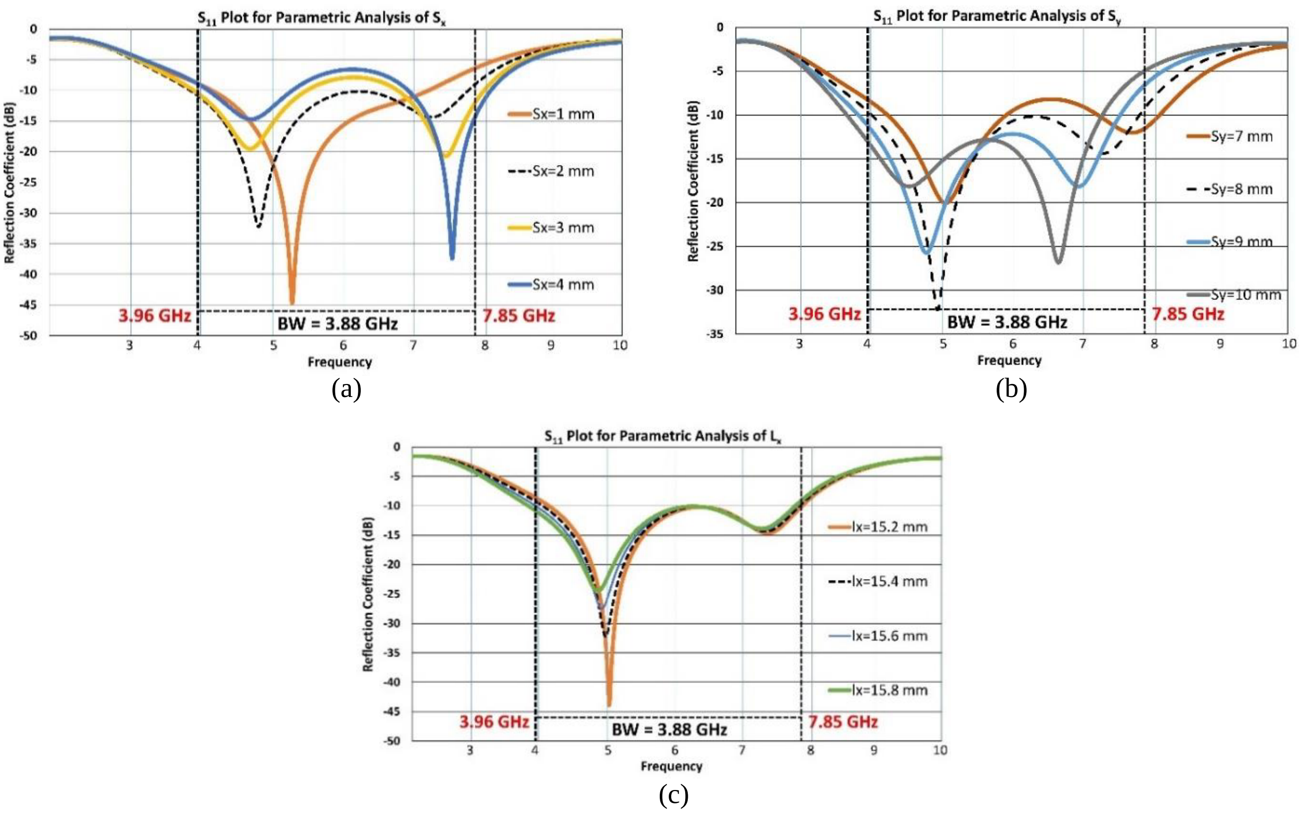

Figure 2. S_{11} versus frequency. (a) For variation in S_x. (b) For variation in S_y. (c) For variation in L_x.

When the value of L_x is varied during the parametric analysis from 15.2 mm to 15.8 mm in step of 0.2 mm, it is observed that the resonating frequency in S_{11} plot varies slightly. Moreover, the maximum bandwidth is achieved when the value of L_x is 15.4 mm. The S_{11} plot has two lows near 4.9 GHz and 7.5 GHz, and the bandwidth obtained is around 3.88 GHz which covers C band and has percentage bandwidth of 65.70%.

2.1. Antenna with PRS with Parasitic Patches

Figure 3(a) shows PRS with parasitic patch placed on top of the Antenna 1. Fig. 3(b) shows the fabricated structure of the Antenna 1. The PRS with parasitic patch is also fabricated using an FR4 substrate with relative permittivity of 4.4. Fig. 3(c) shows the design of PRS with parasitic patches. The waves emerging from PRS are in phase with normal direction. If the field pattern of the antenna is $f(\alpha)$, and the reflection coefficient of PRS is $\rho e^{j\psi}$, then the normalised electric field E and power S

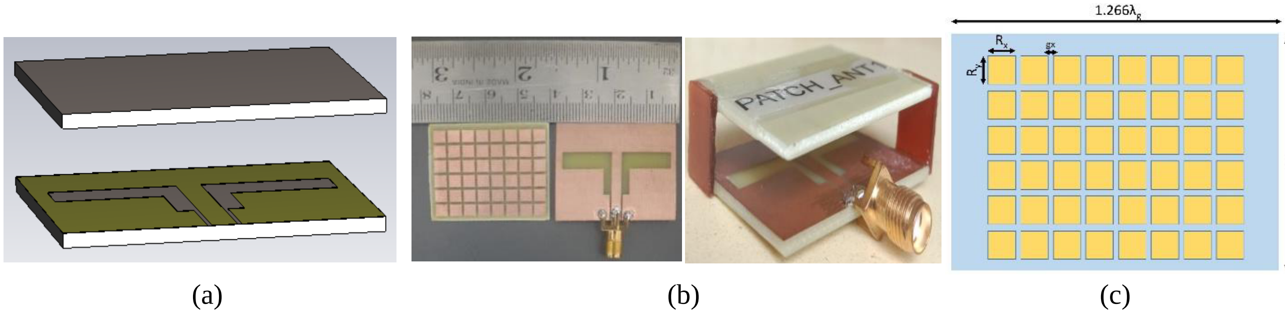

Figure 3. Antenna 1 with PRS with parasitic patch design. (a) Simulated antenna structure. (b) Fabricated antenna structure. (c) PRS with parasitic patches.

are given by Equation (3) [15].

$$|E| = \sqrt{S} = \sqrt{\frac{1-\rho^2}{1+\rho^2-2\rho\cos\Phi}}\, f(\alpha) \tag{3}$$

where Φ is the phase difference between the waves emerging from the PRS.

The gain of the antenna depends upon the aperture area of the antenna and in phase radiated waves from the PRS. The gain and bandwidth are given by Equation (4) [15, 16].

$$G = \frac{(1+\rho)}{(1-\rho)} \text{ and Bandwidth } = \frac{\Delta f}{f_o} = \frac{\left(\frac{\lambda}{2\pi L_r}\right)(1-\rho)}{\rho^{0.5}} \tag{4}$$

Equation (5) gives the value of L_r which is the resonant distance between the CPW-fed antenna and PRS [15].

$$L_r = \frac{\varphi_R}{\pi}\frac{\lambda}{4} + N\frac{\lambda}{2} \text{ Where } \varphi_R + \psi_R - \left(\frac{2\pi}{\lambda}\right)2L_r = 2N\pi \quad N = 0, 1, 2\ldots \tag{5}$$

The value of phase shift $\psi_R = 0$ and a PRS with $\varphi_R = \pi$ would result in a resonant cavity with thickness approximately $\lambda/4$.

Figure 4(a) shows S_{11} plot for parametric analysis for variation in patch size, i.e., Rx and Ry. The optimised values of Rx and Ry are selected as 3.75 mm ($\lambda_g/8$). Fig. 4(b) shows S_{11} plot for the parametric analysis for variation in distance of the patch from antenna, i.e., the best results are obtained for $dx = 7.5$ mm ($\lambda_g/4$). Fig. 4(c) shows S_{11} and gain plot for variations in gap (gx) between the two PRS patches. With increase in gap between the patches, the gain decreases while bandwidth slightly improves. The optimised value of gap (gx) selected between the patches is 0.5 mm. The S_{11} plot shown has a percentage bandwidth of 72.42% (4.44 GHz).

2.2. Miniaturization of Antenna with PRS with Parasitic Patches

Antenna 2 is miniaturized by reducing the width of Antenna 1 as shown in Fig. 5(a). Antenna 2 has the dimension of $0.682\lambda_g \times 0.99\lambda_g \times 0.053\lambda_g$. The equivalent circuit as shown in Fig. 5(b) is a mirror symmetrical circuit. Hence, the distribution of current on left hand side (LHS) of feed line would be same as right hand side (RHS) of feed line. The dominant mode TM_{10} which is excited is the same on LHS and RHS of CPW-fed slot antenna. The antenna impedance is a very important factor for any communication system performance. The antenna impedance is often a critical factor that limits antenna bandwidth. The reflection coefficient S_{11} is calculated using the following formula in Equation (6) [33].

$$S_{11} = \frac{Za - Zo}{Za + Zo^*} \text{ and SWR} = \frac{1+S_{11}}{1-S_{11}} \tag{6}$$

where Za is the antenna impedance, and Zo is the characteristic impedance. The typical requirement for antenna operation is $20\log_{10}|S_{11}| \le -10$ dB and SWR ≤ 2.

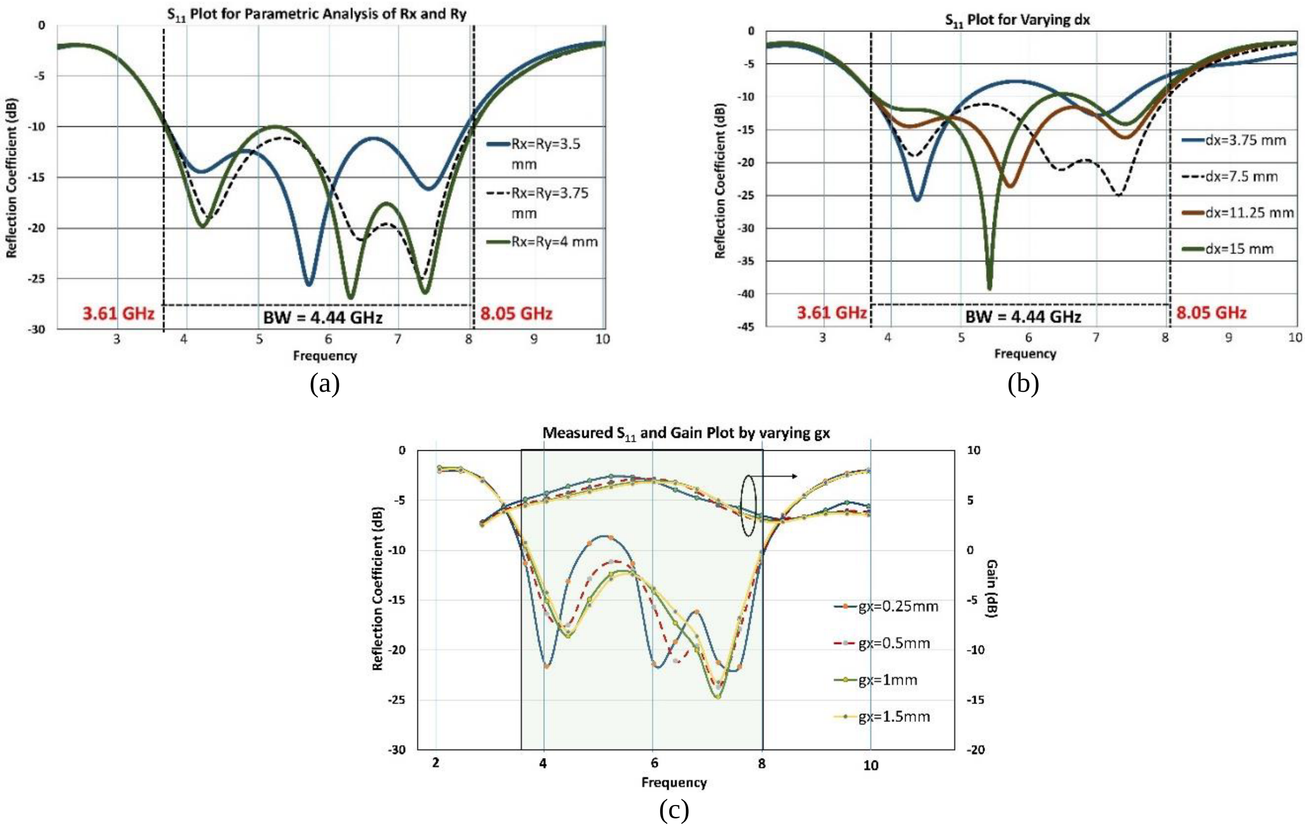

Figure 4. Parametric analysis of PRS with parasitic patches (a) S_{11} plot for variation in Rx and Ry, (b) S_{11} plot for variation in dx, (c) S_{11} and gain plot for variation in gx.

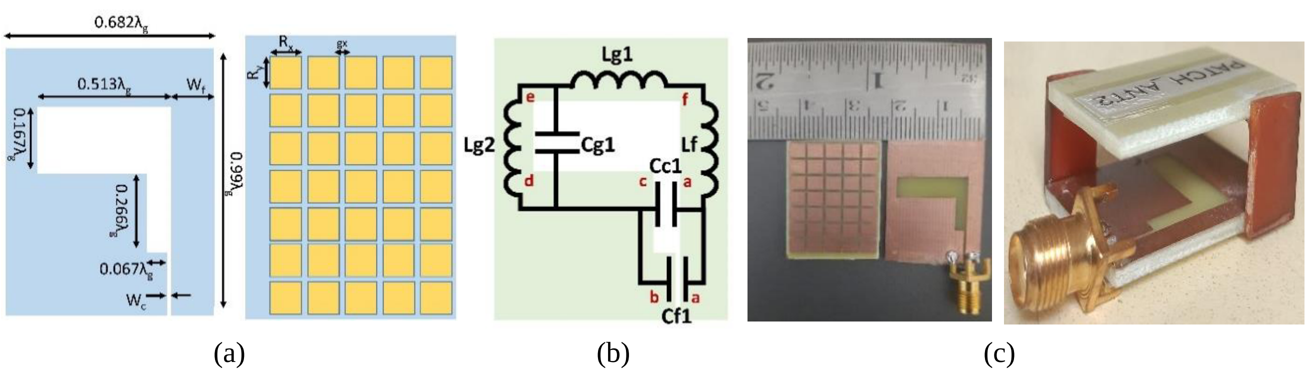

Figure 5. Antenna design. (a) Antenna 2 geometry. (b) Antenna 2 equivalent circuit. (c) Antenna 2 fabricated structure.

The current in the antenna and antenna impedance are given by Equation (7) and Equation (8) [33].

$$I\left(t\right) = \frac{1}{Za}\operatorname{Cos}\left(2\pi ft - \frac{\pi}{180}\varphi\right) \text{ Where } \varphi \text{ is phase angle} \tag{7}$$

$$Za = \frac{Pr + Pd + 2j\omega(W_m - W_e)}{0.5I\left(t\right)I(t)^*} \tag{8}$$

From Equations (7) and (8), both impedance and current mutually depend on each other and on the frequency. At resonance the value of current flowing in the antenna is maximum while the impedance is minimum. W_m and W_e are the average values of magnetic and electric energies in the near-field region.

At resonance the values of magnetic and electric energies are equal, and the antenna reactance becomes zero, which usually occurs when antenna width is close to multiples of $\lambda/2$.

Figure 5(c) shows the fabricated structure of Antenna 2. Antenna 2 is fabricated using FR4 with a thickness of 1.6 mm and dielectric constant of 4.4. Figure 6 shows S_{11} plot of the miniaturized antenna, and the bandwidth of Antenna 2 without PRS is 3.29 GHz with percentage bandwidth of 49.51%. The bandwidth improves to 3.89 GHz with improved percentage bandwidth of 59.80% by placing PRS with parasitic patches on top of Antenna 2. There is a shift in resonance frequency due to the change in size of the antenna, and the gain of the antenna also gets reduced as aperture size of antenna is reduced. Size reduction of 46.50% is achieved which covers almost the entire C band.

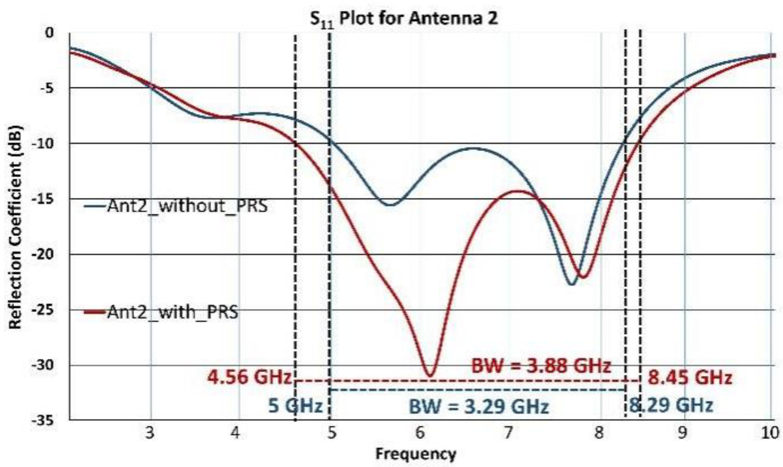

Figure 6. S_{11} versus frequency plot for Antenna 2 with and without PRS with parasitic patches.

2.2.1. Characteristic Mode Analysis for Antenna 2

Characteristic Mode Analysis (CMA) provides an insight into the physical phenomena of an antenna of any arbitrary shape. This facilitates the analysis, synthesis, and optimization of the antenna. By solving a generalized eigenvalue problem involving the impedance matrix of the Method of Moments (MoM), a set of orthogonal eigen-currents together with their associated eigenvalues are obtained. Due to the orthogonality of the eigen-currents, the total current on the surface of the conductor can be expanded into those modes. The eigenvalues provide information about the radiating behaviour of the associated mode. Also, the quantities modal significance MS_n and characteristic angle α_n can be calculated, which are related to the eigenvalue λ_n by Equation (9) [34, 35].

$$\mathrm{MS}_n = \frac{1}{\sqrt{1 + |\lambda_n|^2}} \quad \text{and} \quad \alpha_n = 180^\circ - \arctan(\lambda_n) \tag{9}$$

Modes with characteristic angles near 180° are effective radiators, while those with characteristic angles near 90° or 270° are ineffective radiators [35].

Figure 7 shows characteristic mode analysis for Antenna 2 along with PRS with parasitic patches at 5.8 GHz. Fig. 7(a) shows the plot for modal significance, characteristic angle versus frequency. Mode 1 is the dominating mode at 5.8 GHz with the value of 0.9942, while for mode 2 the value is 0.9821, and for mode 3 the value is 0.9790. The characteristic angle for mode 1 is 173.85 while for mode 2 the value is 169.16, and for mode 3 the value is 191.74. Characteristic Mode Analysis is done in CST software by keeping the number of modes as 3 and frequency for mode sorting as 5.8 GHz. Figs. 7(b), (c), and (d) show the distributions of surface current for mode 1, mode 2, and mode 3, respectively at 5.8 GHz. It is found that the distribution of surface current in Antenna 2 and PRS with parasitic patches remains the same.

Figure 8 shows characteristic mode analysis for Antenna 2 along with PRS with parasitic patches at 7.8 GHz. Fig. 8(a) shows the plot for modal significance, characteristic angle versus frequency. Mode 1

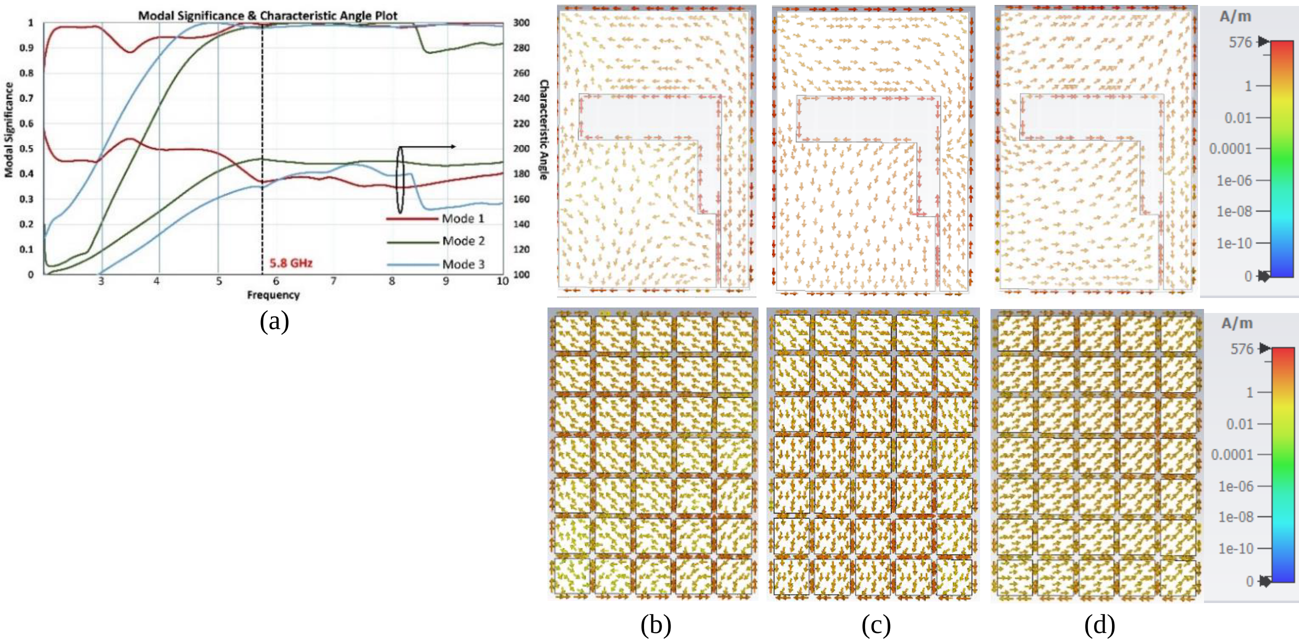

Figure 7. Characteristic mode analysis at 5.8 GHz. (a) Modal significance & characteristic angle. (b) Surface current mode 1 at 5.8 GHz. (c) Surface current mode 2 at 5.8 GHz. (d) Surface current mode 3 at 5.8 GHz.

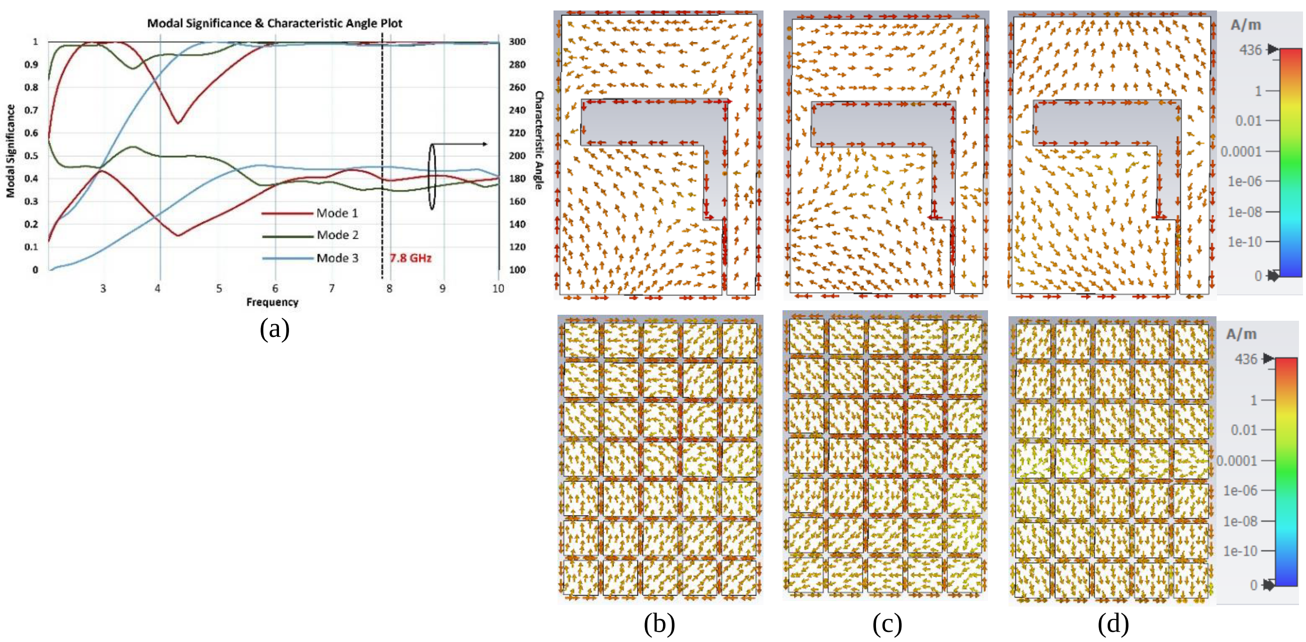

Figure 8. Characteristic mode analysis at 7.8 GHz. (a) Modal significance & characteristic angle. (b) Surface current mode 1 at 7.8 GHz. (c) Surface current mode 2 at 7.8 GHz. (d) Surface current mode 3 at 7.8 GHz.

is the dominating mode at 7.8 GHz with the value of 0.9989, while for mode 2 the value is 0.9982, and for mode 3 the value is 0.9842. The characteristic angle for mode 1 is 182.67° while for mode 2 the value is 171.20°, and for mode 3 the value is 190.17°. Characteristic Mode Analysis is done in CST software by keeping number of modes as 3 and frequency for mode sorting as 7.8 GHz. Figs. 8(b), (c), and (d) show the distributions of surface current for mode 1, mode 2, and mode 3, respectively, at 7.8 GHz. It is found that the distribution of surface current in Antenna 2 and PRS with parasitic patches remain same.

It is clearly seen that the dominating mode over the complete bandwidth for Antenna 2 with PRS with parasitic patches is mode 1. Since the distributions of the current in Antenna 2 and PRS with parasitic patches are the same, also the concentration of current is more when the gap between the patches is less. These cumulatively leads to improvement in the gain.

2.2.2. Measured Results

The proposed antenna was fabricated and tested. The simulation was done using CST studio suite 2021. The reflection coefficient measurement was done using Agilent 8722ET vector network analyser (VNA) at IIT, Bombay. The radiation pattern measurement was done at BITS Pilani, Goa using an anechoic chamber facility with standard horn antenna. The measured results judiciously agree with

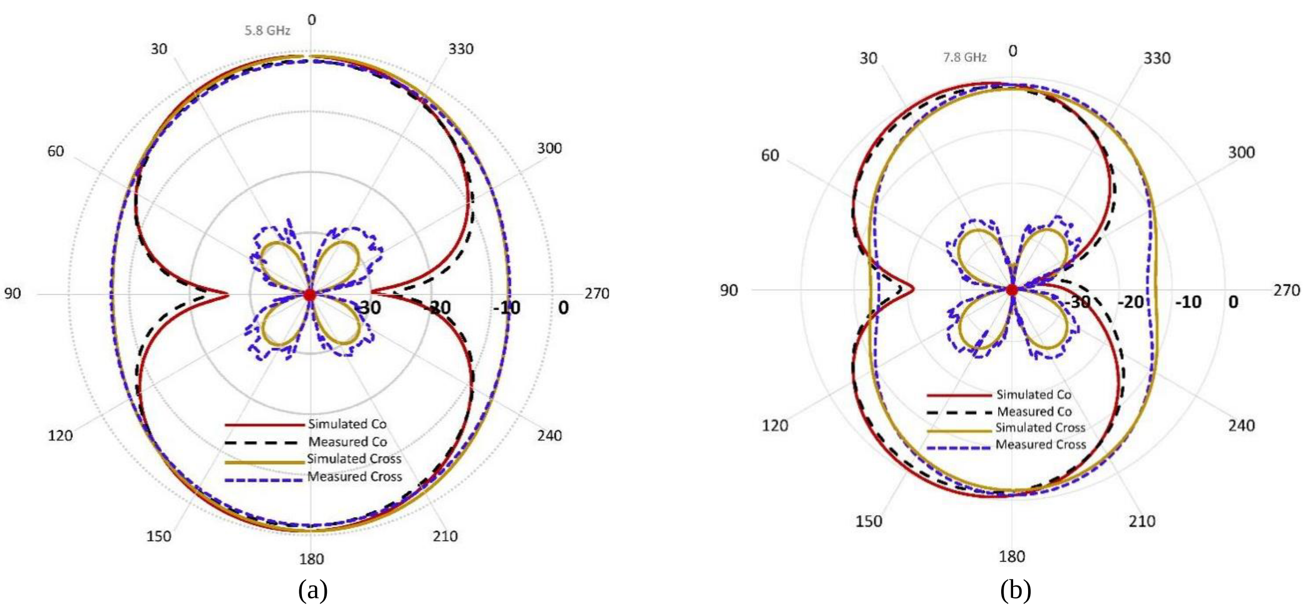

Figure 9. Simulated and measured radiation pattern in E and H plane (a) 5.8 GHz, (b) 7.8 GHz.

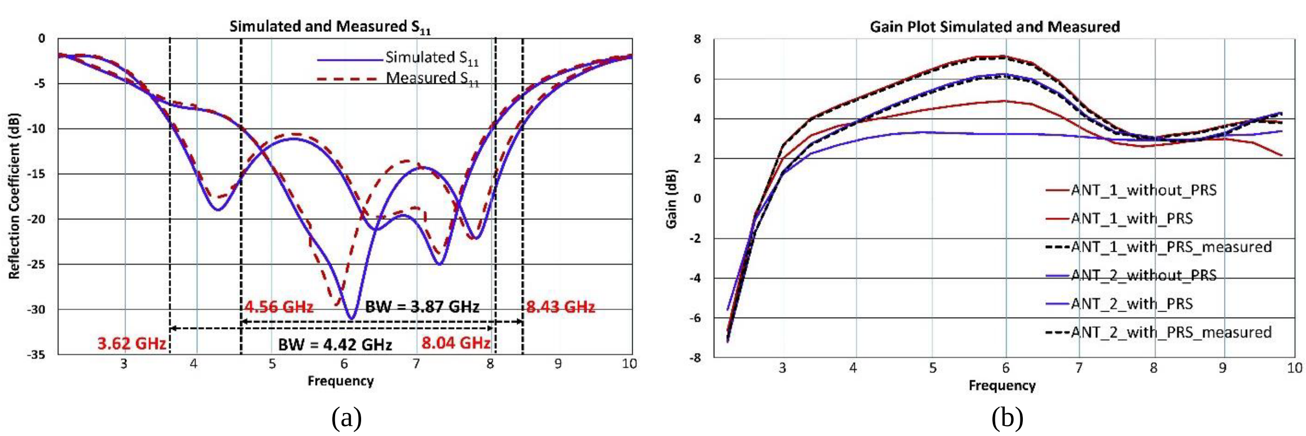

Figure 10. Simulated and measured results for Antenna 1 and Antenna 2 with and without PRS (a) S_{11} versus frequency, (b) gain versus frequency.

the simulated ones. The small variation in the simulated and measured results may be attributed to fabrication error.

The normalised radiation pattern is as shown in Fig. 9. The bidirectional radiation pattern is simulated and measured for Antenna 2 at 5.8 GHz and 7.8 GHz, respectively. The cross polarization measured at 6.08 GHz is -26.39 dB and -24.01 dB at 7.8 GHz in H plane, and cross polarization is < -40 dB in E plane.

The simulated and measured S_{11} plot and the gain plot are as shown in Figs. 10(a) and (b), respectively. The measured bandwidth for Antenna 1 with PRS is 4.42 GHz with percentage bandwidth of 75.81% while the bandwidth of Antenna 2 is 3.87 GHz with a percentage bandwidth of 59.58%. The simulated gains for Antenna 1 and Antenna 2 without PRS are 4.89 dBi and 3.37 dBi. With PRS with parasitic patches placed on top of the Antenna 1, the simulated and measured gains for Antenna 1

Table 1. Comparison with existing results.

Ref. No.	Antenna Size, Material Used, Epsilon Value	Frequency	BW	% BW	Gain
[22]	$0.34\lambda_0 \times 0.34\lambda_0 \times 0.32\lambda_0$ (Antenna with PRS on top and bottom) FR4 4.4	4.43–8.44 GHz (PRS on Top) 4.48–8.59 GHz (PRS on Top and Bottom)	4.01 GHz 4.11 GHz	62.31% 62.89%	5.16 dBi 5.61 dBi
[26]	$0.95\lambda_0 \times 0.95\lambda_0 \times 0.05\lambda_0$ (Single Layer Single Side Multiple Substrate) Rogers RO4003C 3.55	9.13–11.4 GHz	2.27 GHz	22.11%	8.4 dBi
[27]	$1.07\lambda_0 \times 1.07\lambda_0 \times 0.06\lambda_0$ (Single Layer Single Side Multiple Substrate) FR-4 4.4	3.26–5.84 GHz	2.58 GHz	56.7%	11.1 dBi
[28]	$0.47\lambda_0 \times 0.47\lambda_0 \times 0.025\lambda_0$ (Single Layer Single Side Multiple Substrate) FR-4 4.4	3.6–6.1 GHz	2.5 GHz	51.54%	7.87 dBi
[29]	$0.675\lambda_0 \times 0.72\lambda_0 \times 0.036\lambda_0$ (Single Layer Double Side Multiple Substrate) FR-4 4.4	6.5–8.3 GHz	2.05 GHz	24.32%	6.25 dBi
[30]	$1.03\lambda_0 \times 0.78\lambda_0 \times 0.021\lambda_0$ (Single Layer Double Side with lumped elements Multiple Substrate) FR-4 4.4	8.15–13.2 GHz	5.05 GHz	47.31%	7.8 dBi
[31]	$0.75\lambda_0 \times 1.05\lambda_0$ Thickness $0.13\lambda_0$ (Double Layer Single Side on Multiple Substrate) Rogers 5880 2.2	5.85–10.52 GHz	4.67 GHz	57.10%	8.8 dBi
[32]	$1.28\lambda_0 \times 1.28\lambda_0 \times 0.68\lambda_0$ (Double Layer Single Side Multiple Substrate) FR4 4.4	8.2–12.5 GHz	4.1 GHz	44.00%	13 dBi
[36]	$2.1\lambda_0 \times 2.1\lambda_0 \times 0.57\lambda_0$ (Double Layer Single Side Multiple Substrate) Rogers 2.2	7.9–11 GHz	3.1 GHz	32.80%	13.67 dBi
PW	$0.76\lambda_0 \times 0.6\lambda_0 \times 0.032\lambda_0$ (Antenna 1 with PRS) FR4 $0.41\lambda_0 \times 0.6\lambda_0 \times 0.032\lambda_0$ (Antenna 2 with PRS) FR4 4.4	3.62–8.04 GHz 4.56–8.43 GHz	4.42 GHz 3.87 GHz	75.81% 59.58%	7.03 dBi 6.12 dBi

PW — Proposed Work

obtained are are 7.14 dBi and 7.03 dBi, respectively. The simulated and measured gains obtained for Antenna 2 with PRS with parasitic patches placed on top are 6.24 dBi and 6.12 dBi, respectively. The Antenna provides a flat gain response with variation in gain < 3 dBi for complete band.

Figure 11 shows the antenna radiation efficiency for Antenna 1 and Antenna 2. The average radiation efficiency for Antenna 1 is 89.91% while for Antenna 2 it is 90.89%. The radiation efficiency gets improved when PRS with parasitic patches are placed on the top of the antenna. Antenna 1 radiation efficiency improves to 90.40% while for Antenna 2 the radiation efficiency improves to 92.19% for complete range of bandwidth.

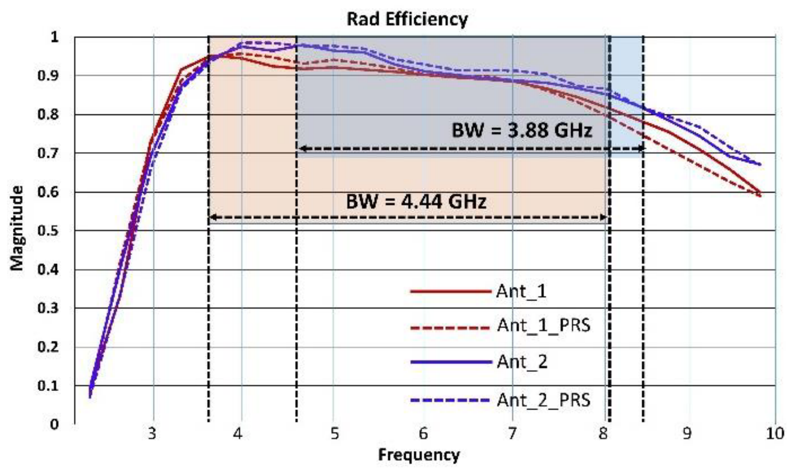

Figure 11. Simulated radiation efficiency of Antenna 1 and Antenna 2 with and without PRS.

The proposed antenna structure is compared with the reported antennas as mentioned in Table 1. The proposed antenna structure has more gain than the antenna in [22]. The proposed antenna has larger bandwidth and % bandwidth than antennas in [26–29, 36]. The proposed antenna has larger bandwidth than the antennas in [30–32]. The size of the proposed antenna is smaller than the antenna in [27, 32, 36].

3. CONCLUSION

A bidirectional wide-band CPW-fed slot antenna with PRS with parasitic patches for improvement in gain, bandwidth, and efficiency is designed and validated. Wide-band performance has been achieved with bands of 4.42 GHz and 3.87 GHz, with percentage bandwidth of 75.81% and 59.58% and average radiation efficiency of 90.40% and 92.19% for Antenna 1 and Antenna 2 with PRS with parasitic patches, respectively. There is considerable gain improvement with gains of 7.03 dBi and 6.12 dBi, respectively for Antenna 1 and Antenna 2 with PRS with parasitic patches. The gain variation is < 3 dB over a complete band making it a flat gain antenna. Miniaturization of 46.50% is achieved by using the symmetrical circuit approach. The presented structure has wide applications in C band due to its wide-band bidirectional nature. The measured results validate the design and concept.

REFERENCES

1. Huynh, T. and K.-F. Lee, "Single-layer single-patch wideband microstrip antenna," *Electronics Letters*, Vol. 31, No. 16, 1310–1312, 1995.
2. Wong, K.-L. and W.-H. Hsu, "Broadband triangular microstrip antenna with U-shaped slot," *Electronics Letters*, Vol. 33, No. 25, 2085–2087, 1997.
3. Guo, Y. X., K. M. Luk, and K. F. Lee, "L-probe proximity-fed short-circuited patch antennas," *Electronics Letters*, Vol. 35, No. 24, 2069–2070, 1999.

4. Tong, K. F., K. M. Luk, K. F. Lee, and R. Q. Lee, "A broad-band U-slot rectangular patch antenna on a microwave substrate," *IEEE Trans. Antennas Propag.*, Vol. 48, No. 6, 954–960, 2000.
5. Yen, M.-H., P. Hsu, and J.-F. Kiang, "Analysis of a CPW-fed slot ring antenna," *Proc. APMC 2001 Int. Conf.*, 1267–1270, 2001.
6. Tehrani, H. and K. Chang, "Multifrequency operation of microstrip-fed slot-ring antennas on thin low-dielectric permittivity substrates," *IEEE Trans. Antennas Propag.*, Vol. 50, No. 9, 1299–1308, Sep. 2002.
7. Gao, G.-P., B. Hu, and J.-S. Zhang, "Design of a miniaturization printed circular-slot UWB antenna by the half-cutting method," *IEEE Antennas and Wireless Propag. Lett.*, Vol. 12, 567–570, May 2013.
8. Li, Z., "Miniaturized design of a CPW-fed slot antennas using slits," *2017 Sixth Asia-Pacific Conference on Antennas and Propagation (APCAP)*, Oct. 2017.
9. Ripin, N., A. A. Sulaiman, N. Emileen, et al., "Miniaturization of printed monopole antenna through fractal geometry and partial cutting methods for UHF application," *2015 International Conference on Computer, Communications, and Control Technology (I4CT)*, Apr. 2015.
10. Salih, A. A. and M. S. Sharawi, "A dual band highly miniaturized patch antenna," *IEEE Antennas and Wireless Propag. Lett.*, Vol. 15, 1783–1786, Mar. 2016.
11. Wheeler, H. A., "Fundamental limitations of small antennas," *Proc. IRE*, Vol. 35, No. 12, 1479–1484, Dec. 1947.
12. Chu, L. J., "Physical limitations on omnidirectional antennas," *J. Appl. Phys.*, Vol. 19, 1163–1175, Dec. 1948.
13. Hansen, R. C., "Fundamental limitations in antennas," *Proc. IEEE*, Vol. 69, 170–182, Feb. 1981.
14. McLean, J. S., "A re-examination of the fundamental limits on the radiation Q of electrically small antennas," *IEEE Trans. Antennas Propag.*, Vol. 44, 672–676, May 1996.
15. Trentini, G. V., "Partially reflecting sheet arrays," *IRE Trans. Antennas Propag.*, Vol. 4, No. 4, 666–671, Oct. 1956.
16. Feresidis, A. P. and J. C. Vardaxoglou, "High gain planar antenna using optimised partially reflective surfaces," *Proc. Inst. Elect. Eng. Microw. Antennas Propag.*, Vol. 148, No. 6, 345–350, Dec. 2001.
17. Foroozesh, N. A. and L. Shafai, "Investigation into the effects of the patch-type FSS superstrate on the high-gain cavity resonance antenna design," *IEEE Trans. Antennas Propag.*, Vol. 58, No. 2, 258–270, Feb. 2010.
18. Alexopoulos, N. and D. Jackson, "Fundamental superstrate (cover) effect on printed circuit antennas," *IEEE Trans. Antennas Propag.*, Vol. 32, No. 8, 807–816, Aug. 1984.
19. Lee, R. Q. and K. F. Lee, "Experimental study of the two-layer electromagnetically coupled rectangular patch antenna," *IEEE Trans. Antennas Propag.*, Vol. 38, No. 8, 1298–1302, Aug. 1990.
20. Egashira, S. and E. Nishiyama, "Stacked microstrip antenna with wide bandwidth and high gain," *IEEE Trans. Antennas Propag.*, Vol. 44, No. 11, 1533–1534, Nov. 1996.
21. Jagtap, S. D., R. K. Gupta, N. Chaskar, S. U. Kharche, and R. Thakare, "Gain and bandwidth enhancement of circularly polarized MSA using PRS and AMC layers," *Progress In Electromagnetics Research C*, Vol. 87, 107–118, 2018.
22. Mehta, A. M., S. B. Deosarkar, and A. B. Nandgaonkar, "Gain and bandwidth enhancement of a CPW-fed bidirectional dumbbell shaped slot antenna using PRS," *Progress In Electromagnetics Research Letters*, Vol. 107, 159–167, 2022.
23. Vaidya, A. R., R. K. Gupta, S. K. Mishra, et al., "Right-hand/left-hand circularly polarized high-gain antennas using partially reflective surfaces," *IEEE Antennas and Wireless Propag. Lett.*, Vol. 13, 431–434, Mar. 2014.
24. Jagtap, S., C. Anjali, and C. Nayana, et al., "A wideband microstrip array design using RIS and PRS layers," *IEEE Antennas and Wireless Propag. Lett.*, Vol. 17, 509–512, Mar. 2018.
25. Foroozesh, A. and L. Shafai, "2-D truncated periodic leaky-wave antennas with reactive impedance surface ground," *Proc. IEEE AP-S Int. Symp.*, 15–18, Albuquerque, NM, Jul. 9–14, 2006.

26. Liao, H.-P. and S.-Y. Chen, "Bandwidth and gain enhancement of CPW-fed slot antenna using a partially reflective surface formed by two-step tapered dipole unit cells," *2019 IEEE Asia-Pacific Microwave Conference (APMC)*, 2019.
27. Zhou, E., Y. Cheng, F. Chen, H. Luo, and X. Li, "Low-profile high-gain wideband multi-resonance microstrip-fed slot antenna with anisotropic metasurface," *Progress In Electromagnetics Research*, Vol. 175, 91–104, 2022.
28. Kumar, A., A. De, and R. K. Jain, "Gain enhancement using modified circular loop FSS loaded with slot antenna for sub-6 GHz 5G application," *Progress In Electromagnetics Research Letters*, Vol. 98, 41–48, 2021.
29. Paik, H., S. K. Mishra, C. M. Sai Kumar, and K. Premchand, "High performance CPW fed printed antenna with double layered frequency selective surface reflector for bandwidth and gain improvement," *Progress In Electromagnetics Research Letters*, Vol. 102, 47–55, 2022.
30. Bhattacharya, A., B. Dasgupta, and R. Jyoti, "Design and analysis of ultrathin X-band frequency selective surface structure for gain enhancement of hybrid antenna," *International Journal of RF and Microwave Computer-Aided Engineering*, e22505, Nov. 2020.
31. Cheng, Y.-F., X. Ding, X. Xu, X. Zhong, and C. Liao, "Design and analysis of a bow-tie slot-coupled wideband metasurface antenna," *IEEE Antennas and Wireless Propag. Lett.*, Vol. 18, No. 7, 1342–1346, Jul. 2019.
32. Kanjanasit, K. and C. Wang, "A wideband resonant cavity antenna assembled using a micromachined CPW-fed patch source and a two-layer metamaterial superstrate," *IEEE Trans. on Components, Packaging and Manufacturing Tech.*, Vol. 9, No. 6, 1142–1150, Jun. 2019.
33. Nikolova, N. K., M. Ravan, and R. K. Amineh, "Chapter six — substrate integrated antennas on silicon," *Advances in Imaging and Electron Physics*, Vol. 174, 391–458, 2012.
34. Ethier, J. L. T., and and D. A. McNamara, "Modal significance measure in characteristic mode analysis of radiating structures," *Electronics Letters*, Vol. 46, No. 2, 107–108, Jan. 2010.
35. Newman, E. H., "Small antenna location synthesis using characteristic modes," *IEEE Trans. Antennas Propag.*, Vol. 27, No. 4, 530–531, Jul. 1979.
36. Fang, S., L. Zhang, Y. Guan, et al., "A wideband Fabry-Perot cavity antenna with single-layer partially reflective surface," *IEEE Antennas and Wireless Propag. Lett.*, Vol. 22, 412–416, Feb. 2023.